JACS Au
AN OPEN ACCESS JOURNAL OF THE AMERICAN CHEMICAL SOCIETY

pubs.acs.org/jacsau
Article

Fabrication of An Immunostimulatory Supramolecular Nanomedicine for Potent Cancer Chemoimmunotherapy

Xinyang Yu, Shaolong Qi, Fangfang Cao, Kai Yang, Hongjian Li, Kun Peng, Zhida Liu,* Bing Bai, Marija Buljan,* Xiaoyuan Chen,* and Guocan Yu*

Cite This: JACS Au 2023, 3, 3181−3193

ABSTRACT: Chemoimmunotherapy can boost strong antitumor immune responses by triggering immunogenic cell death (ICD), which highlights a promising prospect in clinical applications. However, current chemoimmunotherapy shows limited efficacy due to the low delivery efficiency and insufficient immunogenicity of available chemotherapeutic drugs. A supramolecular polymeric nanomedicine (Pt-Tu@NP) is herein reported using cucurbit[7]-uril-based host−guest recognition and noncovalent self-assembly. Pt-Tu@NPs have excellent biodistribution and strongly evoke the endoplasmic reticulum stress-mediated ICD of tumor cells, triggering potent antitumor immune responses by promoting dendritic cell (DC) maturation and cytotoxic T cell infiltration. The coordinated butyrate promotes a positive feedback regulation between DCs and $CD8^+$ T cells. Pt-Tu@NPs stimulate immune cold tumors into hot ones, working in synergy with an immune checkpoint blockade to effectively suppress tumor growth and metastasis, which suggests a promising approach for cancer chemoimmunotherapy.

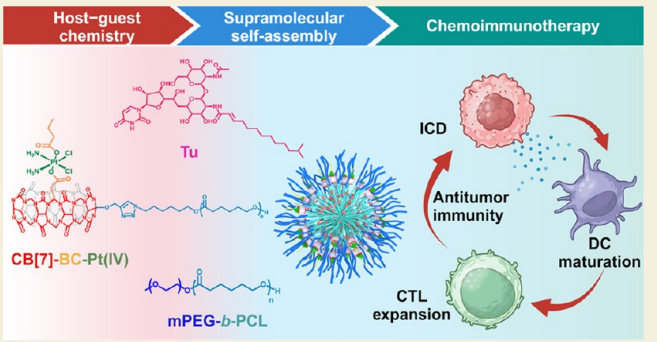

KEYWORDS: *cancer immunotherapy, endoplasmic reticulum stress, immunogenic cell death, host−guest chemistry, supramolecular nanomedicine*

INTRODUCTION

Cancer immunotherapy with immune checkpoint blockade (ICB) has limited curative efficacy for many patients due to poor immunogenicity and inadequate lymphocyte infiltration.[1] An important challenge in cancer research is to identify means for ICB use in conjunction with other treatments that support the conversion of immune cold tumors into hot ones.[2] Some chemotherapeutic drugs, such as doxorubicin and paclitaxel, have shown the capability to elicit immunogenic cell death (ICD)-associated antitumor immunity, emerging as promising options for immunotherapy synergy.[3] Cisplatin (CDDP), the classical first-line drug generally applied in the treatments of various cancers,[4] has been proven to be a booster for programmed cell death-ligand 1 (PD-L1) expression.[5] However, inadequate immunogenic activity of CDDP results in a lack of cytotoxic T lymphocyte infiltration, which is a critical foundation for ICB-mediated antitumor immunity.[6]

Endoplasmic reticulum (ER)-targeted stress makes tumor cells visible to immune system and triggers a strong immune response, promoting ICD-related immunotherapy.[7,8] Intriguingly, ER-stressor tunicamycin (Tu) can compensate for the relatively weak immunogenic signals after CDDP administration. As a corollary, the combination of these two drugs induces ICD more effectively than either of them alone.[9,10] Nevertheless, systemic administration of Tu and CDDP is severely limited due to their poor accumulation and severe side effects.[11,12] Due to their distinct physicochemical properties, the pharmacokinetic behaviors and biodistributions of these two drugs are distinct after intravenous injection, possibly attenuating the therapeutic efficacy and causing severe systemic toxicity. Nanotechnology provides new opportunities to coencapsulate CDDP and Tu into one nanoformulation with an optimized ratio, facilitating the achievement of a synergistic anticancer outcome. More intriguingly, the antitumor efficacy of the developed nanomedicines can be greatly promoted by exploiting the enhanced permeability and retention (EPR) effect, and unwanted side effects derived from the free drugs can also be dramatically avoided.[13,14]

Specifically, supramolecular nanomedicine combines multiple therapeutic elements into a single platform constructed by noncovalent interactions and has received considerable

Received: August 31, 2023
Revised: October 22, 2023
Accepted: October 23, 2023
Published: November 7, 2023

https://doi.org/10.1021/jacsau.3c00515
JACS Au 2023, 3, 3181−3193

Scheme 1. (a) Chemical Structures of BC-Pt(IV), CB[7]-PCL, mPEG-*b*-PCL, and Tu; Schematic Illustration of the Preparation of Pt-Tu@NPs through Host−Guest Interactions and Noncovalent Self-Assembly and (b) Illustration of the Procedure Involving the Antitumor Effect of Pt-Tu@NPs[a]

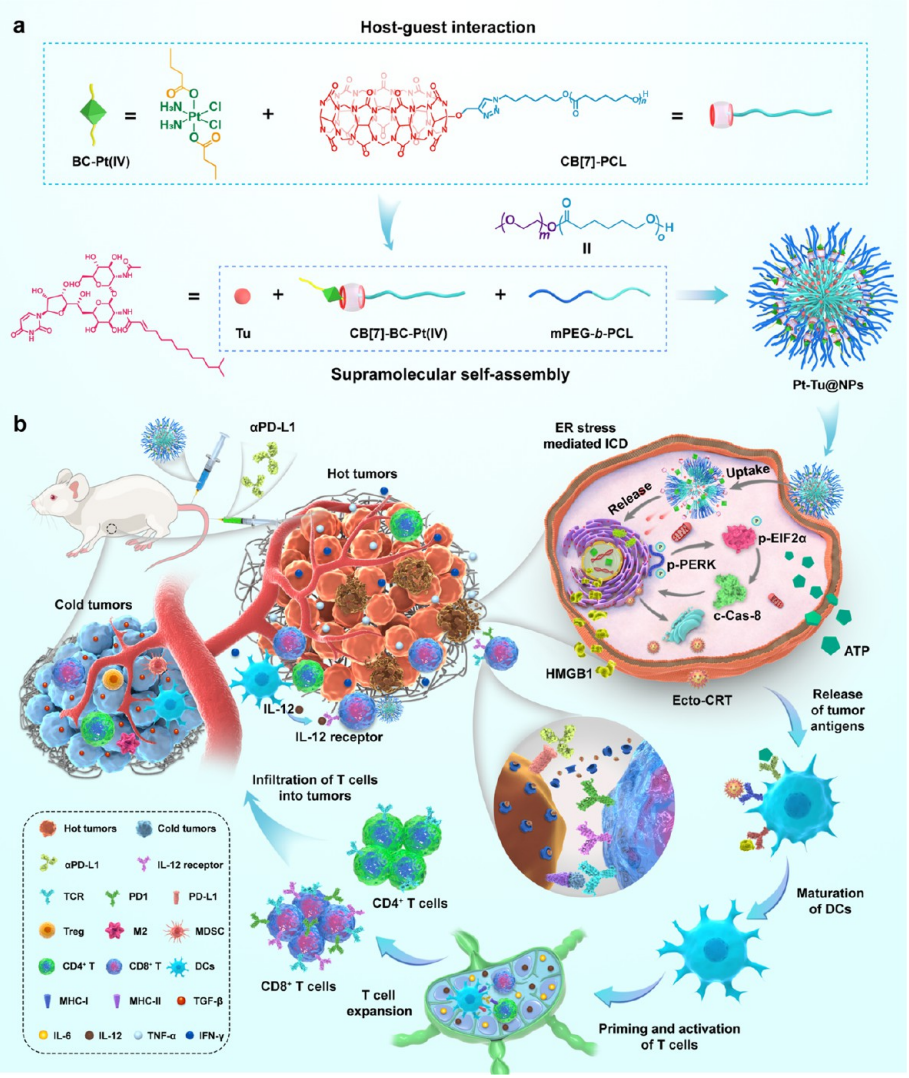

[a]Maturation of DCs is promoted by antigen exposure from dying tumor cells, including CRT exposure, HMGB1 leakage, and ATP secretion. Pt-Tu@NPs evoke ER stress-mediated ICD of tumors to enhance lymphocytic infiltration and transform immune "cold" into "hot" tumors, which lead to an effective tumor suppression and synergism with αPD-L1 therapy.

attention in recent years due to its unparalleled advantages underlined by the dynamic and reversible nature of noncovalent interaction.[15] It is especially suitable for drugs that release and activate at the site of action triggered by specific characteristics of tumor microenvironments. As a result, this may promote tumor inhibition and minimize side effects.[16] Cucurbiturils have been extensively employed to build supramolecular polymers and drug delivery systems because of their rigid structure and high association constant with the guests.[17] Cucurbit[7]uril (CB[7]) with a cavity allows it to encapsulate a variety of chemically and physiologically interesting substances including different hydrophobic chemotherapeutic drugs and their derivatives. Additionally, due to its adaptable properties, CB[7] is a fantastic candidate carrier for the combined delivery of different insoluble chemotherapy drugs.[18]

Here, we report a supramolecular nanomedicine (Pt-Tu@NP) based on CB[7] host−guest recognition and noncovalent self-assembly (Scheme 1). Nanoparticles are prepared through noncovalent self-assembly using CB[7]-modified polycaprolactone (CB[7]-PCL), polyethylene glycol-*b*-PCL (mPEG-*b*-PCL), and Tu as building blocks in which CB[7] forms an inclusion complex with butyric acid (BC)-modified Pt(IV) through host−guest interactions, thus achieving codelivery of BC-Pt(IV) and Tu. Pt-Tu@NPs effectively evoke the ER stress-mediated ICD of tumor cells, enabling active immune responses. Benefiting from prolonged blood circulation and high tumor retention, Pt-Tu@NPs further amplify the ICD effects of tumor cells and promote dendritic cell (DC) maturation, cytotoxic lymphocyte infiltration, and antitumor immune responses. The coordinated butyric acid is proven to be effective in promoting the interaction between DCs and T cells. Furthermore, Pt-Tu@NPs enable synergism in combination with ICB in effectively suppressing tumor growth and metastasis.

https://doi.org/10.1021/jacsau.3c00515
JACS Au 2023, 3, 3181−3193

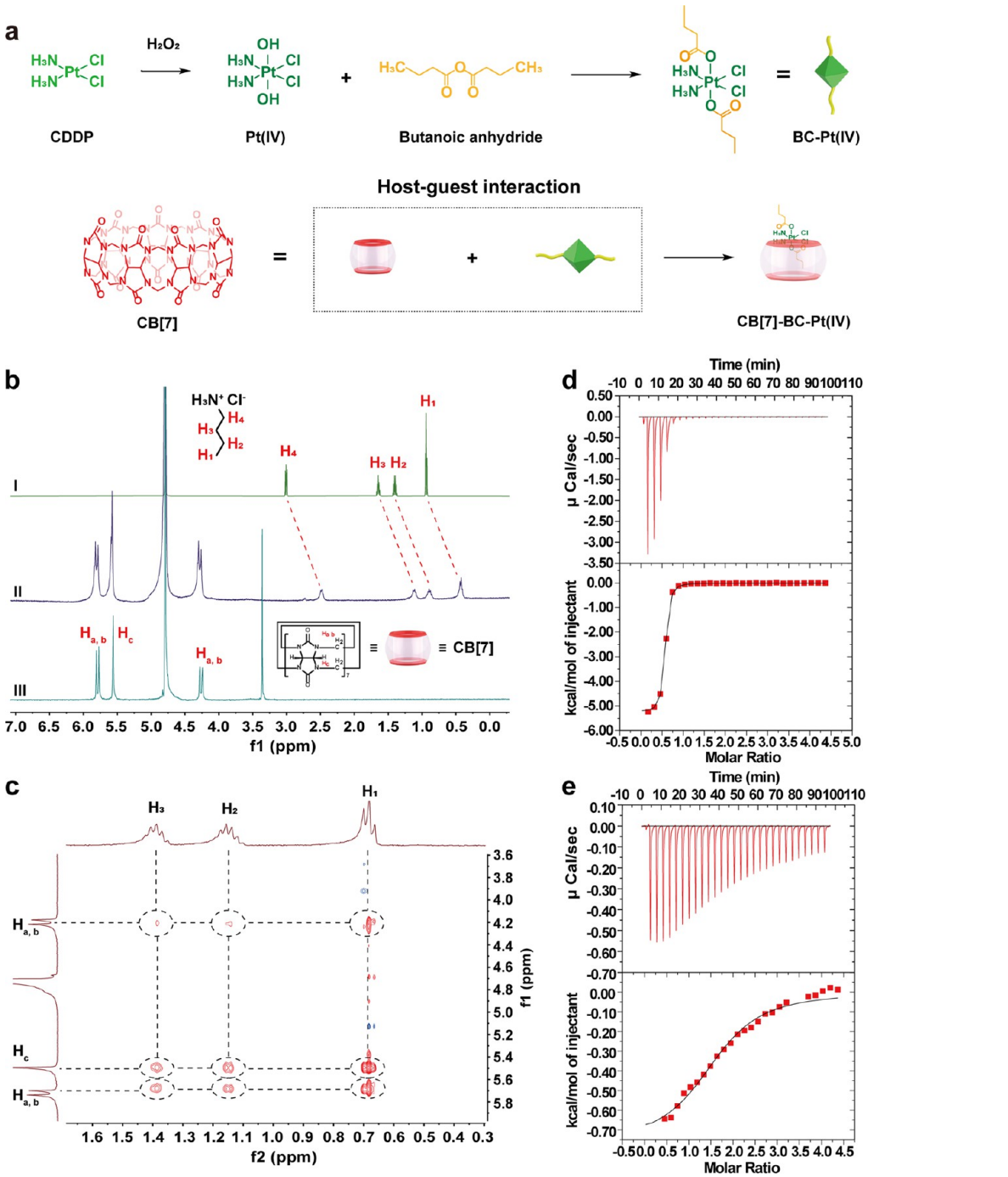

Figure 1. (a) Synthetic routes of BC-Pt(IV) and host–guest complex CB[7]-BC-Pt(IV). (b) ^{1}H NMR spectra of I, M (1.00 mM); II, CB[7] (1.00 mM) and M (1.00 mM); and III, CB[7] (1.00 mM). (c) 2D NOESY spectrum of host–guest complex between CB[7] and M. The ITC results of the host–guest complex between (d) CB[7] and M or (e) CB[7] and CDDP.

RESULTS AND DISCUSSION

Concentration-dependent cytotoxicity was observed for 4T1 cells treated independently with CDDP and Tu. The half-maximal inhibitory concentration (IC_{50}) values of CDDP and Tu were calculated to be 7.94 ± 0.16 and 0.25 ± 0.09 μM, respectively (Figures S1 and S2). Notably, the cytotoxicity of Tu against 4T1 cells was significantly boosted in the presence of CDDP, whose IC_{50} value decreased to 0.05 ± 0.003 μM, implying a synergistic antitumor effect of CDDP and Tu (Figure S3). To improve the encapsulation efficiency and overcome its off-target toxicity, CDDP was oxidized into a Pt(IV) prodrug, whose axial ligands provided attachment points for bioactivity addition and nanocarrier incorporation (Figures 1a and S4).

It should be emphasized that the modification of CDDP did not change the synergistic effects between Tu and BC-Pt(IV). Indeed, the results shown in Figure S5 confirmed that the anticancer efficacy of BC-Pt(IV) was significantly increased in the presence of Tu. The synergistic effect of BC-Pt(IV) and Tu on augmenting ATP release indicated that these dying tumor cells could be immunogenic (Figure S6). Confocal laser scanning microscopy (CLSM) images showed that the

https://doi.org/10.1021/jacsau.3c00515
JACS Au 2023, 3, 3181–3193

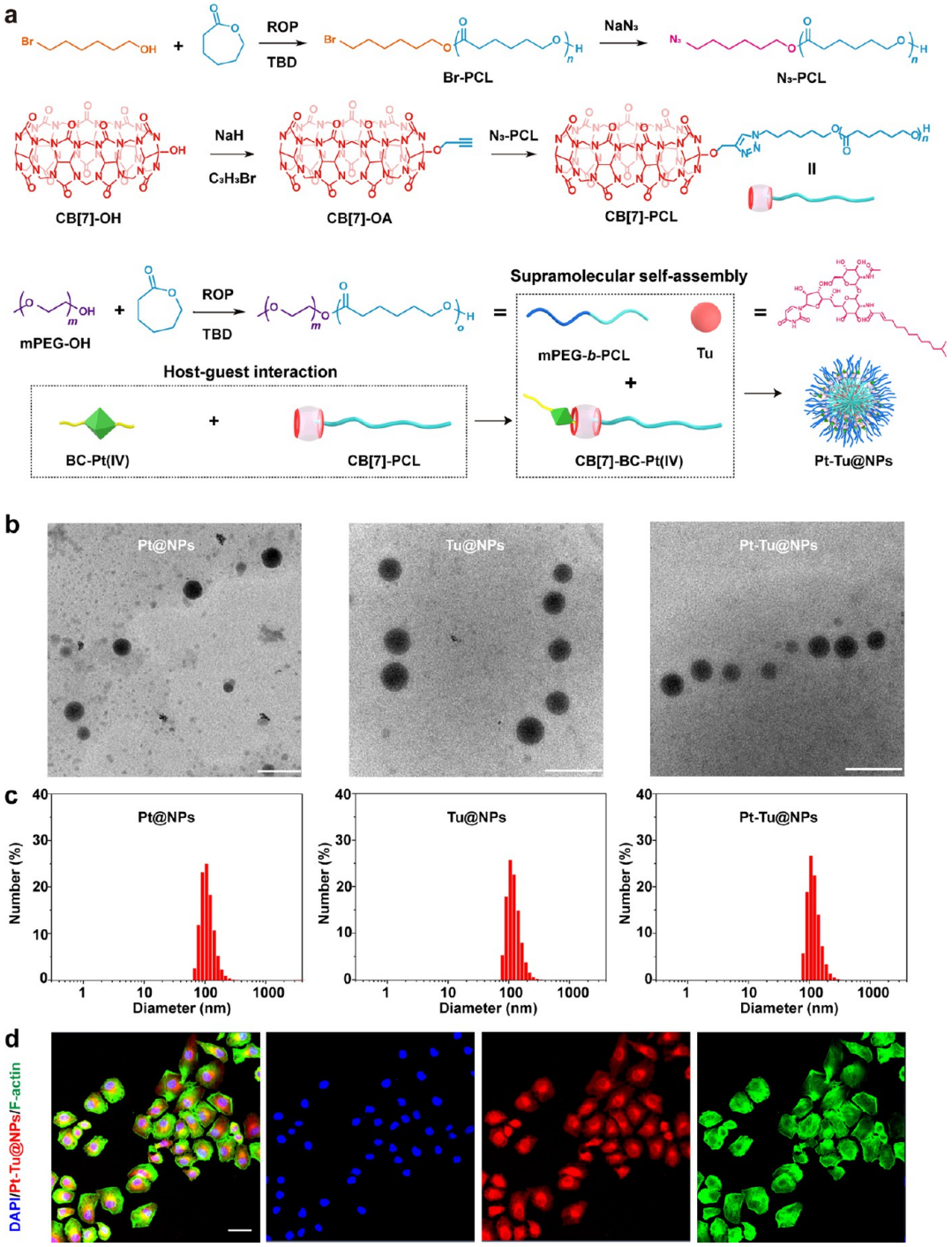

Figure 2. (a) Synthetic routes of CB[7]-PCL and mPEG-*b*-PCL. Preparation of supramolecular nanomedicine Pt-Tu@NPs. (b) TEM images and (c) DLS results of Pt@NPs, Tu@NPs, and Pt-Tu@NPs. (d) CLSM images of 4T1 cells treated with Rhodamine 6G-labeled Pt-Tu@NPs. Nuclei were stained by DAPI, and F-actin was stained by green fluorescence. Scale bar: 20 μm.

combined treatment triggered a remarkable CRT exposure on the surface of 4T1 cells, a marker of high cellular stress. In contrast, following the BC-Pt(IV) or Tu treatment alone, fluorescently labeled CRT molecules were mainly distributed in ER and clustered around the nucleus (Figure S7), thus suggesting that BC-Pt(IV) or Tu alone are deficient in inducing ICD. HMGB1 is known as a delayed signal of ICD. It can be recognized by DCs through Toll-like receptor 4 and subsequently promote their maturation and activation.[19] The treatment with BC-Pt(IV) and Tu incited a strong release of HMGB1 from the nucleus of 4T1 breast cancer cells (Figure S8), while BC-Pt(IV) or Tu alone was inefficient in triggering HMGB1 leakage.

The combination of BC-Pt(IV) and Tu successfully evoked strong ER stress responses. In comparison to the BC-Pt(IV) treatment alone, the level of p50 and p90 ATF6 increased by 1.40-fold after receiving BC-Pt(IV) and Tu. The levels of phosphorylated PERK and EIF2α (p-PERK and p-EIF2α) increased by 1.40-fold and those of p18 caspase-8 (p18 Cas-8) by 1.60-fold in the 4T1 cells treated with BC-Pt(IV) and Tu

https://doi.org/10.1021/jacsau.3c00515
JACS Au 2023, 3, 3181−3193

(Figures S9 and S10). These findings demonstrated that BC-Pt(IV) and Tu potentially cooperated with each other and had a synergistic role in promoting CRT exposure through the stress-related PERK pathway. During the ER stress, the cumulative unfolded proteins competitively bind to chaperone GRP78, allowing for the activation of the PERK kinase, which acts as an ER stress sensor protein. Sensitization of PERK causes the phosphorylation of EIF2α and leads to partial activation of caspase-8, which is crucial for releasing ICD-related signals. The cleavage of BAP31 performed by cleaved-caspase-8 can markedly promote CRT exposure through the SNAREs-dependent exocytosis.[20]

Considering its strong binding affinity and excellent biocompatibility, CB[7] was chosen as the host molecule to construct the supramolecular nanomedicine. The hydrophobic butyl group of BC-Pt(IV) penetrated into the cavity of CB[7] to form an inclusion host−guest complex driven by the hydrophobic interactions. Additionally, the cationic -NH_3 groups of BC-Pt(IV) appended on the rim of CB[7] further stabilized the complexation by multiple cation−dipole interactions. Considering the poor solubility of BC-Pt(IV) in aqueous solution, the host−guest complexation between CB[7] and BC-Pt(IV) was first investigated by nuclear magnetic resonance (^{1}H NMR) spectra by using butylamine hydrochloride (M) as a model guest. Due to the formation of inclusion complex, the signals related to the protons shifted upward, and the peaks became broadened upon addition of CB[7] (Figures 1b and S11). 2D NOESY NMR spectrum indicated strong nuclear Overhauser effect (NOE) correlations between the signals related to the protons on M and CB[7], thus suggesting that M penetrated deeply into the cavity of CB[7] (Figure 1c). The association constant (K_a) of this host−guest complex was determined by isothermal titration calorimetry (ITC), which also provided the complexation thermodynamic parameters. The K_a value of this host−guest complex was calculated to be $(2.01 \pm 0.11) \times 10^6$ M^{-1}, indicating that the binding affinity was strong enough to guarantee the encapsulation of BC-Pt(IV) by CB[7] (Figure 1d). Moreover, the enthalpy change was negative while the entropy change was positive; both enthalpy and entropy changes were thus favorable for the host−guest complexation. In addition, ITC measurement indicated the K_a value of the CB[7] and CDDP formulation $(4.49 \pm 0.80) \times 10^4$ M^{-1} (Figure 1e) was much lower than that of CB[7] and BC-Pt(IV). The reduction of BC-Pt(IV) into CDDP significantly weakened the binding affinity and facilitated drug release and its activation inside cells.

CB[7]-PCL was synthesized through a copper-catalyzed click reaction between alkyl-modified CB[7] and azide-modified PCL, which was obtained from a ring-opening polymerization using 6-bromo-1-hexanol as an initiator followed by the reaction with sodium azide. The amphiphilic copolymer mPEG-*b*-PCL that could assist the noncovalent self-assembly was synthesized using mPEG−OH as a macromolecular initiator (Figure 2a). The structures and properties of these compounds were well characterized by gel permeation chromatography and ^{1}H NMR spectra (Figures S11−S16), which demonstrated the successful preparation of the building blocks. Supramolecular nanomedicines were prepared using a nanoprecipitation method, and the polymeric vehicles and anticancer drugs were solubilized in DMSO and gradually dropped into aqueous solution under sonication. Two driven forces were responsible for drug loading: the hydrophobic interactions between PCL segments and the alkyl chain of Tu and the host−guest interactions between BC-Pt(IV) and CB[7].

In order to verify the synergistic anticancer efficacy, three nanomedicines were produced that loaded different therapeutics (Pt@NPs, Tu@NPs, and Pt-Tu@NPs). To identify the optimum proportion of drugs, cytotoxicity profiles of different drug-loaded nanoparticles administered to 4T1 breast cancer cells were detected using a 3-(4′,5′-dimethylthiazol-2′-yl)-2,5-diphenyl tetrazolium bromide (MTT) assay. In the presence of Tu@NPs, Pt@NPs effectively induced cell apoptosis, and the IC_{50} value decreased from 10.5 ± 0.11 μM (Pt@NPs alone) to 1.13 ± 0.04 μM (Figure S17). The viability of cancer cells treated with Pt@NPs (2.00 μM) and Tu@NPs (0.01 μM) was reduced to 36.9% (Figure S18). Benefiting from the strong binding affinity of host−guest complex and relatively low content of Tu, these two drugs were encapsulated in this ratio in the supramolecular nanomedicine. The ratio of BC-Pt(IV) and Tu was controlled to 200:1 for all further investigations by adjusting the original concentration of the drugs during nanoformulation.

The morphology of nanomedicines was investigated by transmission electron microscopy (TEM), and the obtained images indicated the formation of nanoparticulate structures (Figure 2b). The average diameters of Pt@NPs, Tu@NPs, and Pt-Tu@NPs were determined to be 111 ± 6.61, 121 ± 7.65, and 119 ± 5.60 nm, respectively, by dynamic light scattering (DLS). These results were in good agreement with the ones from TEM images (Figure 2c). The produced nanomedicines were stable in PBS, and only negligible changes in diameter were observed after 48 h of incubation (Figure S19). This suggested that the dissociation of nanomedicines could be avoided during blood circulation. Cellular uptake of nanomedicines was monitored using CLSM, where signal originating from Pt-Tu@NPs labeled with Rhodamine 6G was observed in the cytoplasm (Figures 2d and S20), which indicated that Pt-Tu@NPs were efficiently internalized. Time-dependent intracellular uptake of platinum was analyzed by inductively coupled plasma mass spectrometry (ICP-MS). The intracellular platinum continuously increased over time following incubation with Pt@NPs and Pt-Tu@NPs (Figure S21). However, the platinum amount in the BC-Pt(IV) group ascended up to 5.10 ng per 1×10^6 cells at 12 h and then exhibited only a slight increase in the next 12 h. These characterizations indicated that supramolecular nanoformulation effectively enhanced cellular endocytosis, thus facilitating the anticancer efficacy of Pt-Tu@NPs.

The prodrug BC-Pt(IV) can be activated into potent CDDP after cell internalization by intracellular reducing agents, such as glutathione (GSH). Results shown in Figure S22 showed a low leakage (<10%) of BC-Pt(IV) from Pt-Tu@NPs in the absence of GSH, whereas a majority of platinum was found to be released from the nanomedicines in the presence of GSH (5.00 mM) after 24 h incubation. As depicted in Figure S23, nearly 80% of Tu was released after 24 h. Benefiting from strong endocytosis and effective release, cytotoxic effects of nanomedicines against cancer cells were far superior to those of free drugs. As shown in Figure S24, Pt-Tu@NPs were able to initiate a higher apoptosis rate than BC-Pt(IV) or Tu. The IC_{50} value for the combination of BC-Pt(IV) and Tu (0.01 μM) was calculated to be 9.06 ± 0.09 μM, while the value for Pt-Tu@NPs decreased to 1.81 ± 0.02 μM. Overall, this suggested excellent anticancer efficacy of the nanoformulation.

https://doi.org/10.1021/jacsau.3c00515
JACS Au 2023, 3, 3181−3193

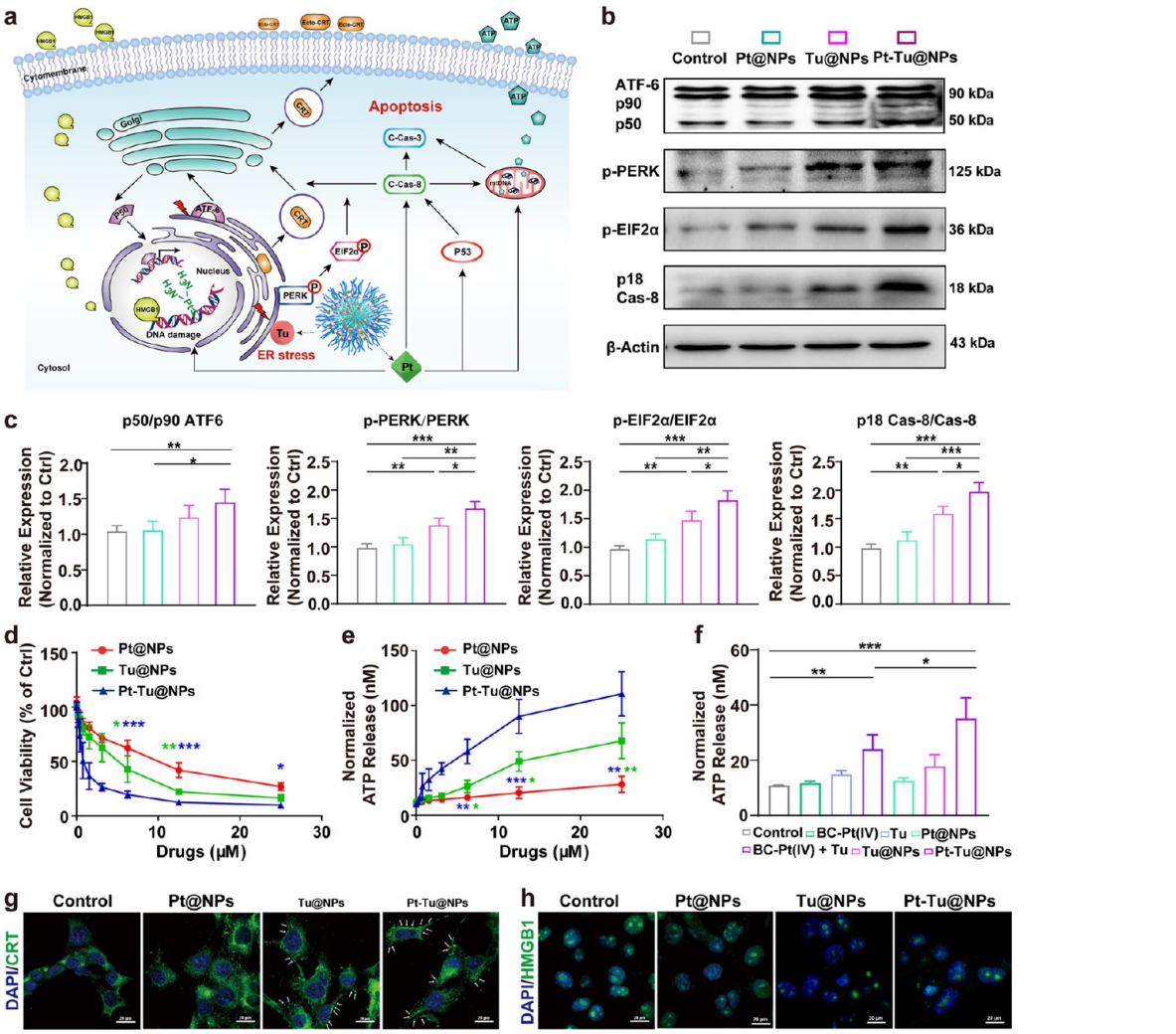

Figure 3. (a) Schematic representation of the underlying mechanisms related to ER stress-mediated ICD of tumor cells by Pt-Tu@NPs. Representative Western blot (b) and normalized level (c) of ER-stress-related proteins from 4T1 cells under different treatments. (d) Cell viability of 4T1 cells after various treatments. (e) ATP content in supernatants from 4T1 cells treated with different nanoagents. (f) ATP content in culture supernatants for 4T1 cells after different treatments. Mean ± SD $^{*}p < 0.05$, $^{**}p < 0.01$, $^{***}p < 0.001$. CLSM determination for the CRT exposure (g) and the location of HMGB1 (h) in 4T1 cells treated with different nanomedicines. The white arrow denoted the membrane localization of CRT. Scale bar = 20 μm.

Endocytosis of Pt-Tu@NPs into tumor cells followed by intracellular degradation led to the release of potent Pt(II) drugs. The translocation of CRT from the ER lumen to the plasma membrane (Ecto-CRT) might require parallel activation of different cellular pathways, including ER stress-mediated PERK/EIF2α/caspase-8 signaling together with the processes that could be elicited by Pt(II), such as DNA damage response (Figure 3a), or changes within intracellular signaling routes.[10] Ratios of p50/p90 ATF6 and p18 Cas-8/Cas-8 exhibited 1.44- and 1.97-fold increases; p-PERK/PERK and p-EIF2α/EIF2α were also enhanced by 1.68 and 1.82 times for 4T1 cells treated with Pt-Tu@NPs, making them the strongest candidates for promoting the ER stress response (Figures 3b,c and S25). As predicted, Pt-Tu@NPs exhibited significantly enhanced cytotoxicity and ATP release from 4T1 cells compared with those of Tu@NPs and Pt@NPs (Figure 3d,e). It was notable that the treatment with Pt-Tu@NPs generated a higher ATP release than that of the naked regimen (BC-Pt(IV) + Tu) (Figure 3f). CRT exposure and HMGB1 release were also obviously higher for the 4T1 cells treated with Pt-Tu@NPs. CLSM images showed a high-caliber membrane localization of CRT and a sharp decrease in the nucleus-located signal of HMGB1 for the 4T1 cells administrated with Pt-Tu@NPs (Figures 3g,h and S26, S27). Flow cytometry analysis revealed similar results of membrane CRT and intranuclear HMGB1 expressions in 4T1 cells when treated with Pt-Tu@NPs nanomedicine (Figure S28), demonstrating that Pt-Tu@NPs efficiently promoted the ER stress-elicited ICD of tumor cells.

The supramolecule-based nanocarriers protected drugs against rapid phagocytosis by the reticuloendothelial system in vivo, thus greatly extending their circulation time. As shown in Figure 4a,b, the administration of Pt-Tu@NPs resulted in a longer drug elimination half-life ($t_{1/2}$) and larger area under curve. Its $t_{1/2}$ was calculated to be 1.54 ± 0.17 h, which was higher than that of free CDDP with a $t_{1/2}$ of 0.36 ± 0.04 h. A near-infrared fluorescent probe, indocyanine green (ICG), was incorporated into Pt-Tu@NPs through coassembly to trace their in vivo delivery behaviors. Pt-Tu@NPs exhibited an excellent tumoral distribution benefiting from the EPR effect,

https://doi.org/10.1021/jacsau.3c00515
JACS Au 2023, 3, 3181−3193

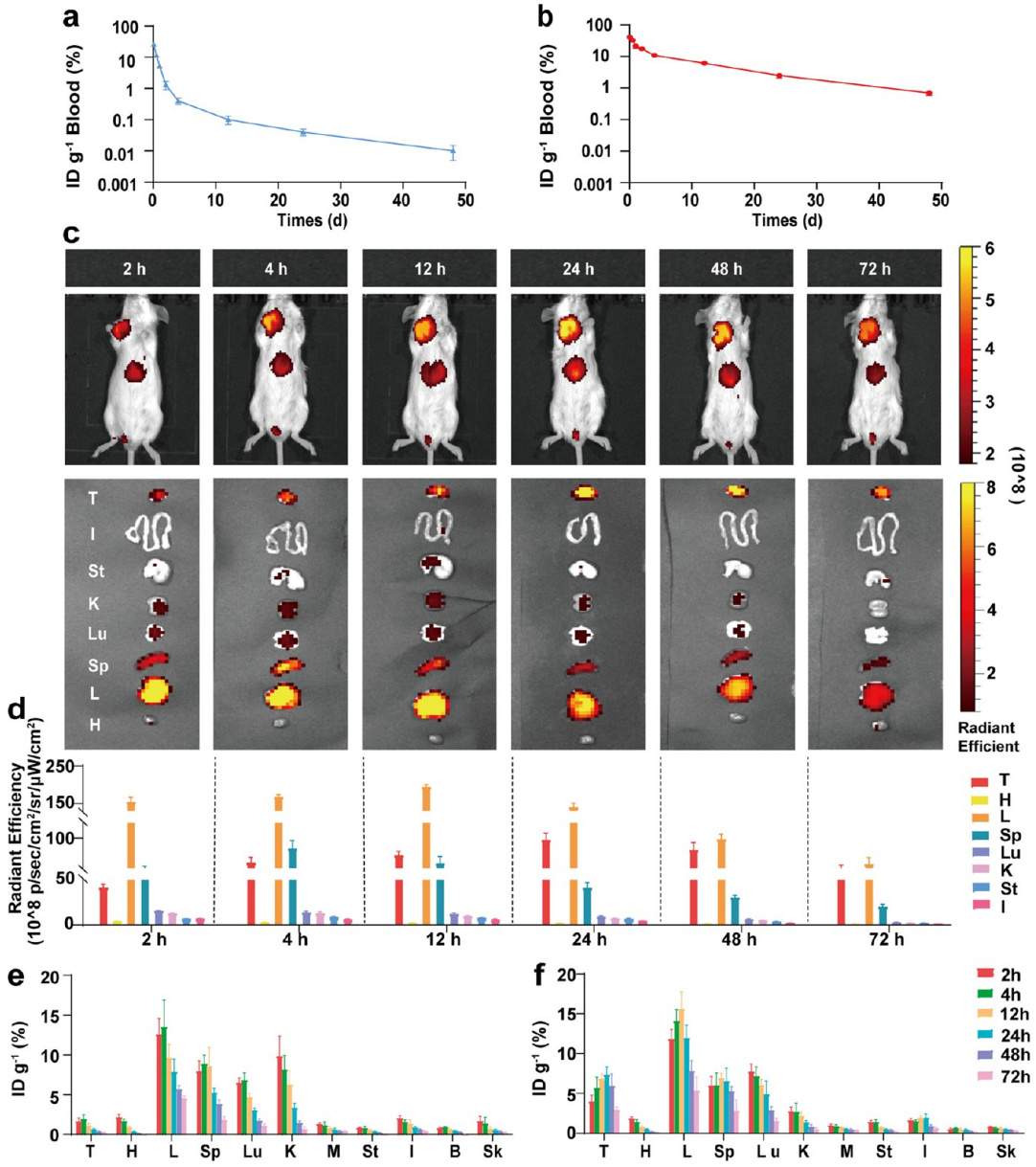

Figure 4. Pharmacokinetic profiles of (a) CDDP and (b) Pt-Tu@NPs determined by ICP-MS after i.v. administration. (c) In vivo fluorescence images of orthotopic 4T1 tumor and the ex vivo of organ biodistribution after administration of Pt-Tu@NPs for 2, 4, 12, 24, 48, and 72 h. (d) Quantification of the fluorescence intensity per organ area. Biodistribution of (e) CDDP and (f) Pt-Tu@NPs at different time points post i.v. injection. Mean ± SD. Tumor (T), heart (H), liver (L), spleen (Sp), lung (Lu), kidney (K), muscle (M), stomach (St), intestine (I), bone (B), and skin (Sk).

and the high contrast signal was clearly observed on the orthotopic 4T1 tumor area with peak accumulation at 24 h postintravenous (*i.v.*) injection (Figure 4c,d). Then, all of the important organs were dissected for ex vivo imaging. Apart from the obvious distribution on tumor, signals had part retention in the metabolic organs (e.g., liver, kidney, and stomach). The signal in the liver was diminished 12 h, but the orthotopic tumor was still clearly visible after 72 h. This suggested good tumor penetration and sustained retention for the better cancer therapy. The intratumoral amount of Pt-Tu@NPs increased from 3.93 ± 0.85%ID g^{-1} at 2 h to 6.80 ± 0.65% and 7.30 ± 1.05%ID g^{-1} at 12 and 24 h post injection, and 2.90 ± 0.40%ID g^{-1} remained in tumors even 72 h later. In contrast, the highest tumor accumulation of CDDP following i.v. injection reached only 1.90 ± 0.60%ID g^{-1} at 4 h and rapidly deceased to 0.23 ± 0.04%ID g^{-1} at 72 h post injection (Figure 4e,f). Moreover, drug content in kidneys of the mice administered with Pt-Tu@NPs was 2.7 3 ± 0.56%ID g^{-1} at 2 h post injection, while the value for CDDP treatment raised to 9.80 ± 2.55%ID g^{-1}, indicating that Pt-Tu@NPs were able to reduce off-target toxicity.

To evaluate the therapeutic efficacy of the supramolecular nanomedicine and its synergism with ICB, 4T1 tumor-bearing mice were treated with the nanomedicine alone or in combination with antibodies against PD-L1 (αPD-L1) (Figure 5a). In vivo antitumor evaluation indicated that the tumor growth was effectively suppressed after the administration of either Pt@NPs, Tu@NPs, or Pt-Tu@NPs, and the corresponding tumor growth inhibition (TGI) was calculated to be 53.2, 62.3, and 78.9%, respectively, which is much higher than

https://doi.org/10.1021/jacsau.3c00515
JACS Au 2023, 3, 3181−3193

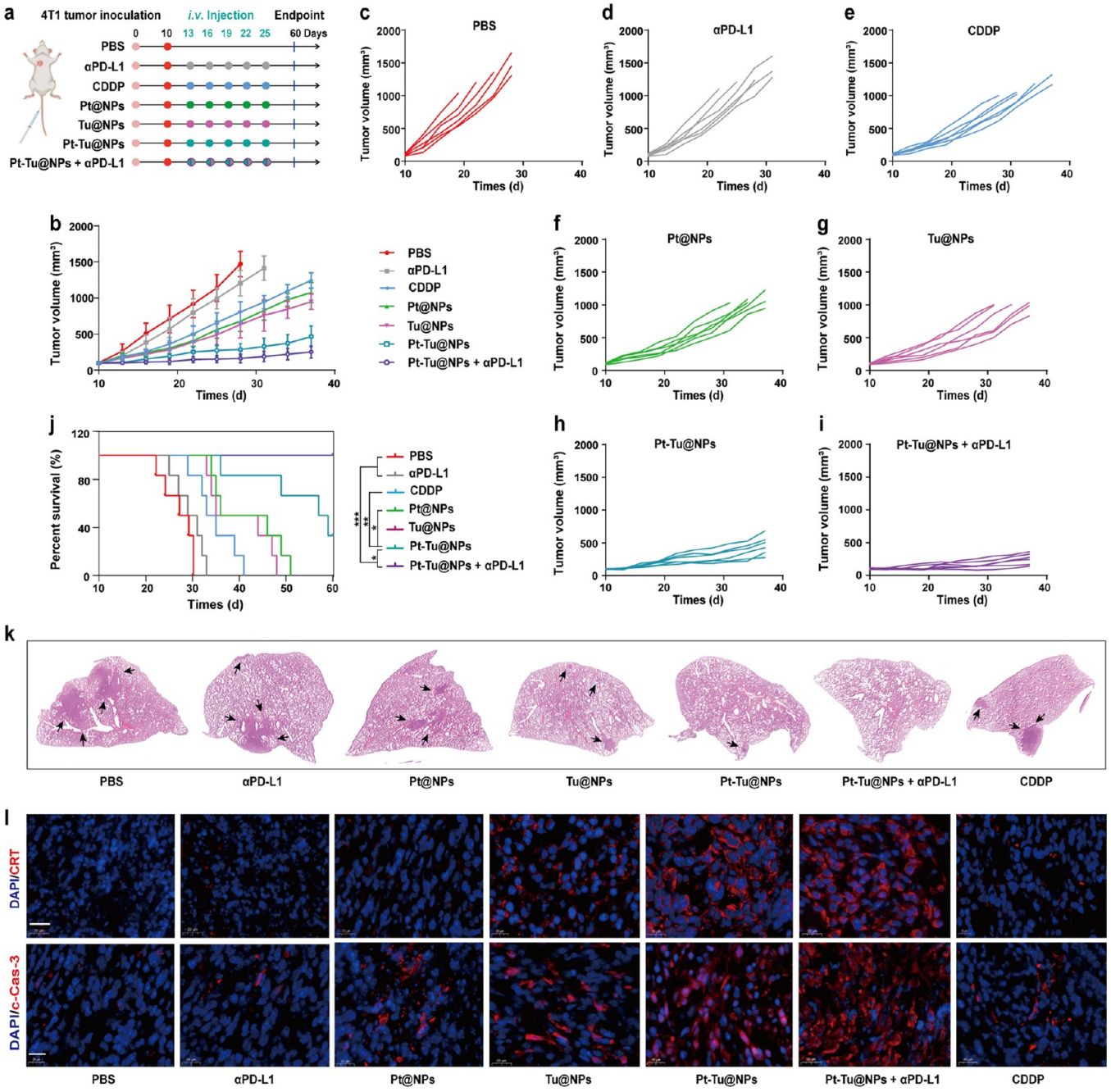

Figure 5. (a) Experimental scheme of the in vivo antitumor therapy. (b) Average tumor volume, (c–i) individual tumor growth curves, and (j) survival curves of the mice after various treatments. (k) Hematoxylin and eosin (H&E) staining of the lung tissues from the mice after different administrations. (l) Representative CLSM images of CRT and c-Cas-3 positive cells in tumor tissues from the mice after indicated treatments, Scale bar = 50 μm.

the TGI measured after the CDDP administration, which was 40.5% (Figures 5b,c–i and S29). Notably, the antitumor effect achieved by αPD-L1 alone was marginal, with a TGI value of 9.11%. In contrast, the combination of Pt-Tu@NPs and αPD-L1 dramatically suppressed tumor growth, as measured by a TGI value of 82.6%. Excitingly, the administration of Pt-Tu@NPs + αPD-L1 induced a fairly obvious central necrosis (Figure S30). The average survival time for mice treated with Pt-Tu@NPs was 58 days, whereas the survival time for PBS-treated mice was 28 days and for CDDP-treated mice 34 d. This further supported the excellent therapeutic value of Pt-Tu@NPs. For the mice treated with a single αPD-L1, the median survival time was 30 d. However, all of the mice treated with Pt-Tu@NPs + αPD-L1 remained alive at the defined end point of 60 d, suggesting the combination therapy significantly extended survival time benefiting from its superior therapeutic performance (Figure 5j). The supramolecular nanomedicine also exhibited excellent antimetastatic effect, where fewer pulmonary cancer cell clusters and reduced metastatic foci in lung tissue were observed for the mice administrated with Pt-Tu@NPs + αPD-L1 (Figures 5k and S31). These findings indicated that Pt-Tu@NPs significantly enhanced the anticancer performances and synergized with ICB immunotherapy, thus amplifying response to chemoimmunotherapy and

https://doi.org/10.1021/jacsau.3c00515
JACS Au 2023, 3, 3181–3193

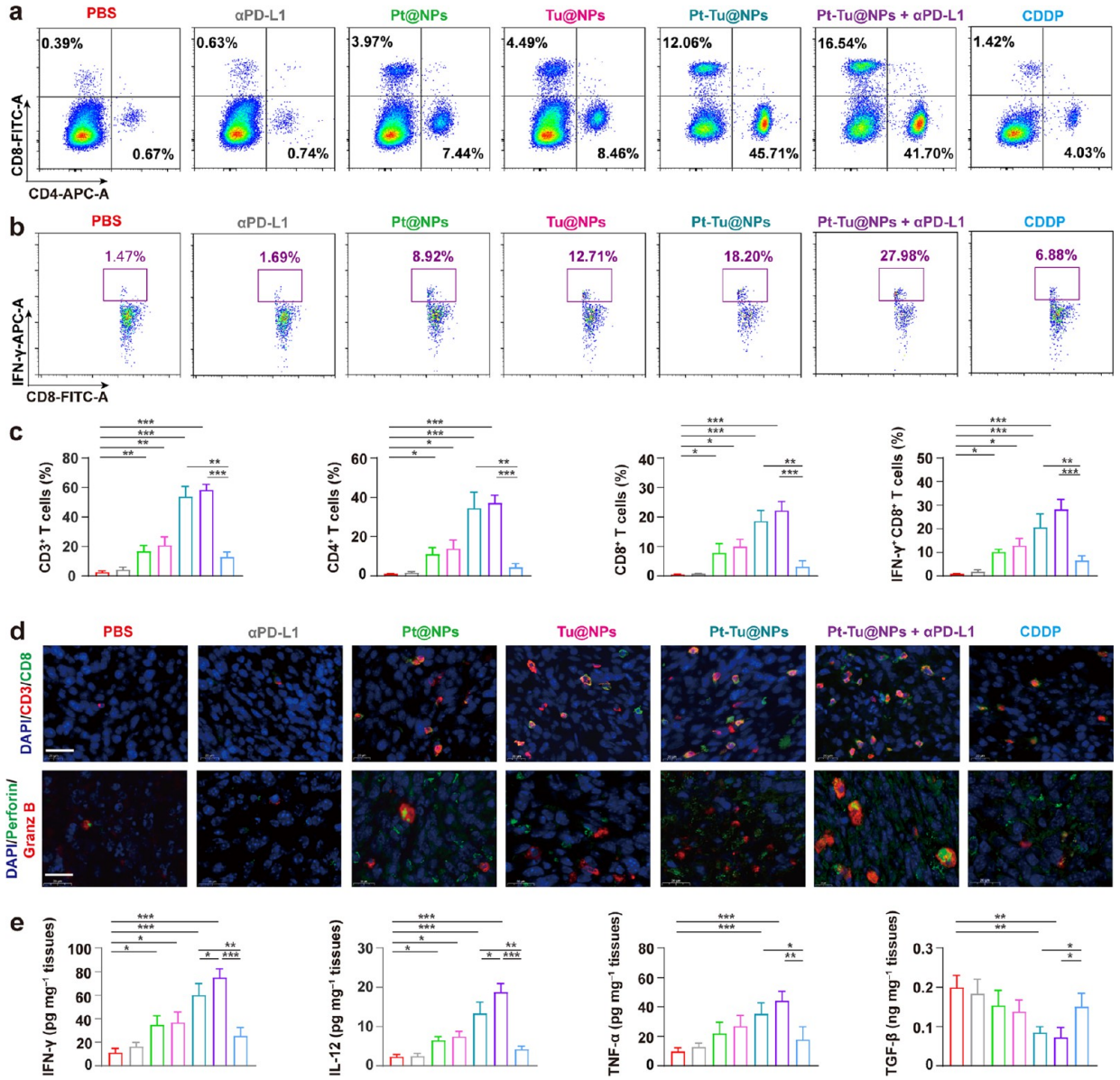

Figure 6. (a) Fow cytometry data of $CD4^+$ and $CD8^+$ T cells in 4T1 tumors. (b) Flow cytometry analysis of IFN-γ^+CD8^+ T cells in tumors. (c) Quantitative analysis of $CD3^+$, $CD4^+$, and $CD8^+$ T cells. (d) CLSM images of $CD3^+CD8^+$ T cells, perforin, and granzyme B secretion in tumor tissues from mice after various treatments, Scale bar = 20 μm. (e) Concentrations of IFN-γ, IL-12, TNF-α, and TGF-β in tissue lysates from mice after different treatments. Mean ± SD $^*p < 0.05$, $^{**}p < 0.01$, $^{***}p < 0.001$.

preventing tumor metastasis for the treatment of triple-negative breast cancer in a mouse model. Although body weights of the mice that were administered Pt-Tu@NPs were slightly reduced, partially due to the shrinkage of tumors, no significant difference was shown among the treatment groups, suggesting minimal systemic toxicity of the nanoformulation (Figure S32).

It is worth noting that cancer chemoimmunotherapy is particularly effective when ICD is induced due to a strong antitumor immune response. Indeed, the evident exposure of CRT was observed in tumor sites for the mice administered with Pt-Tu@NPs + αPD-L1, with intense red signals predominantly distributed on the cell surfaces (Figures 5l and S33). The transfer of CRT from ER to membrane increased the recognition by immunocytes, which was favoring the killing of cancer cells (Figures S34−S40). Cleaved-caspase-3 (c-Cas-3) is the active form of caspase-3 and is known to be a critical executive molecule for cells undergoing ICD and entering apoptosis. As shown in Figure 5l, we found that the fluorescent c-Cas-3 signals were intensively increased for the mice treated with Pt-Tu@NPs and Pt-Tu@NPs + αPD-L1, in particular after the latter treatment. In comparison, only weak signals of c-Cas-3 were observed in tumor tissues from the mice treated with CDDP, Pt@NPs and Tu@NPs (Figures S41−S47).

CRT exposure on cancer cells provides immune recognition by DCs and stimulates DC maturation and the secretion of cytokines, thus enhancing their antigen presentation to promote T cell priming and differentiation.[21] We found here that the maturation markers (CD80 and CD86) of DCs from draining lymph nodes were strongly upregulated in the mice injected with Pt-Tu@NPs (Figures S48−S55). DC maturation is significantly influenced by the proinflammatory cytokine IL-6.[22] Mice treated with Pt-Tu@NPs showed elevated IL-6 levels

https://doi.org/10.1021/jacsau.3c00515
JACS Au 2023, 3, 3181−3193

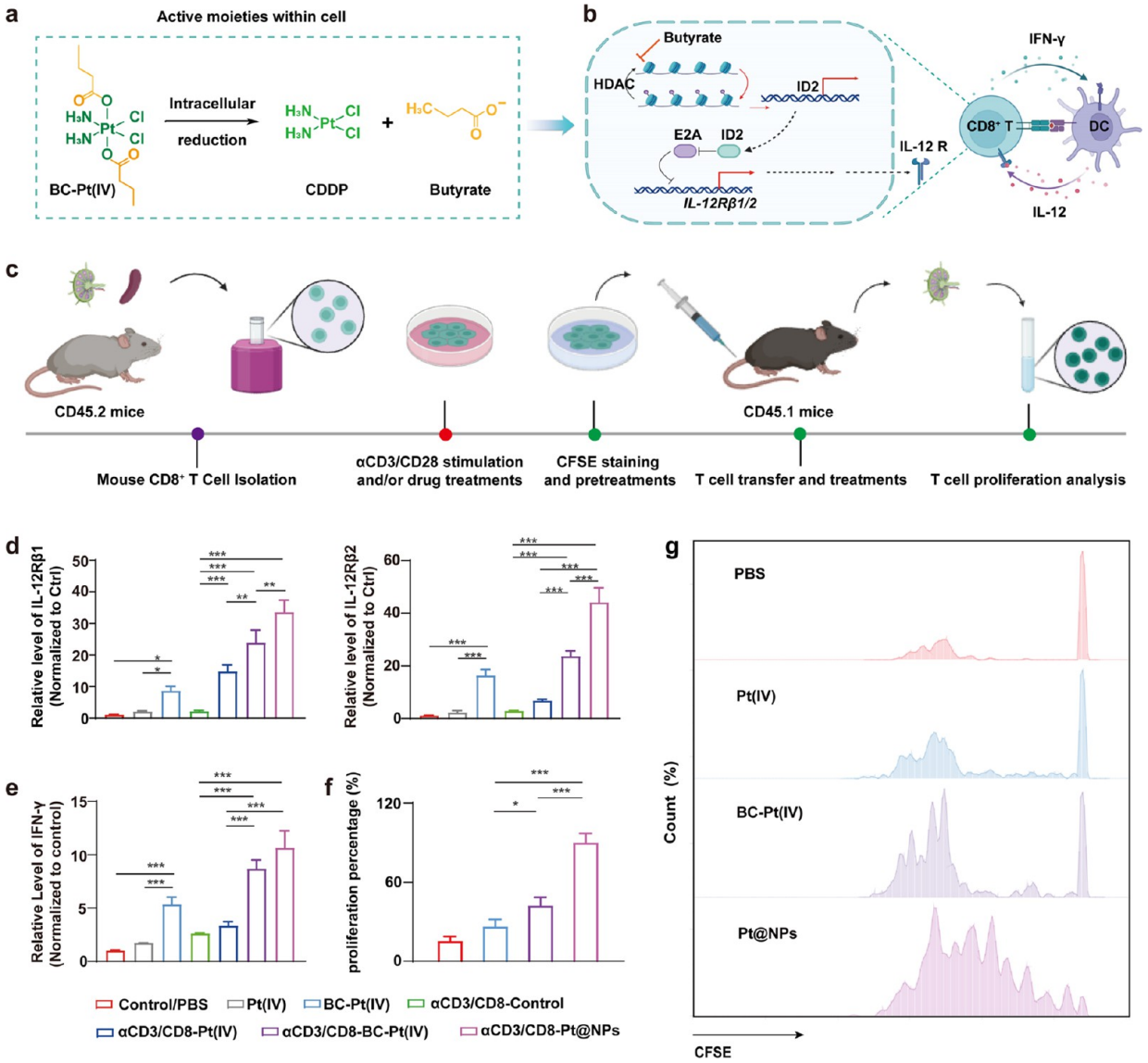

Figure 7. (a) Illustration of the intracellular degradation of BC-Pt(IV). (b) Model for how the coordinated butyrate improves the IL-12 receptor expression and promotes a positive-feedback regulation between DCs and CD8$^+$ T cells. (c) Schematic representation of T cell isolation and CFSE proliferation assay in vivo. (d) qRT-PCR analysis of *IL-12Rβ1* and *IL-12Rβ2* among CD8$^+$ T cells after different ex vivo treatments. (e) Relative level of IFN-γ in the supernatants derived from CD8$^+$ T lymphocytes following different ex vivo stimulations. (f) Representative histograms and (g) percentages of CFSE-labeled proliferative CD8$^+$ T cells. Mean ± SD *p < 0.05, **p < 0.01, ***p < 0.001.

in draining lymph nodes that were 5.58 times higher than those in mice treated with PBS (Figure S56). IL-12 produced by DCs promotes T lymphocyte activation and proliferation, which aid in the immune response against tumors.[23] Pt-Tu@NPs treatment in mice elevated IL-12 up to 3.66 times more than PBS treatment (Figure S57). These findings verified that Pt-Tu@NPs could effectively boost the DC maturation, which plays an essential role in fostering adaptive immunity against cancer.

Since CD4$^+$ and CD8$^+$ T lymphocytes play a pivotal role in the immune surveillance of tumors, populations of infiltrating T cells in tumor tissues from the mice that received different treatments were analyzed by CLSM and flow cytometry. The proportions of intratumoral CD4$^+$ T cells from the mice administered with αPD-L1, CDDP, Pt@NPs, and Tu@NPs were measured to be 1.51%, 4.28%, 11.0%, and 13.8%, respectively (Figure 6a,c). The trafficking of intratumoral CD4$^+$ T cells increased to 34.4% and 37.1% for the mice treated with Pt-Tu@NPs and Pt-Tu@NPs + αPD-L1. These data demonstrated that Pt-Tu@NPs could effectively promote the infiltration of effector T cells into tumors. Moreover, the frequencies of infiltrating CD8$^+$ and IFN-γ^+CD8$^+$ T cells were measured to be 3.13% and 7.75%, 9.87% and 10.2%, 7.49% and 12.8% for the mice treated with CDDP, Pt@NPs, and Tu@NPs. The intratumoral flux of CD8$^+$ and IFN-γ^+CD8$^+$ T cells were elevated to 18.6% and 20.5% in mice treated with Pt-Tu@NPs, and further increased to 22.1% and 28.1% when combined with αPD-L1 (Figure 6a–c, Figures S58–S71). These findings suggested that Pt-Tu@NPs effectively promoted the homing and trafficking of cytotoxic CD8$^+$ T cells, which were synergistically strengthened by ICB therapy.

Consistent with flow cytometry results, CLSM images showed more infiltration of CD8$^+$ T cells in tumor sites for the mice treated with Pt-Tu@NPs and Pt-Tu@NPs + αPDL1 (Figures 6d and S72–S75). Notably, the granzyme/perforin-dependent cytotoxic effect is one of the critical markers of

https://doi.org/10.1021/jacsau.3c00515
JACS Au 2023, 3, 3181–3193

tumor killing by $CD8^+$ T cells.[24] As illustrated in Figure 6d, the expansion of tumor-infiltrating perforin and granzyme B double-positive $CD8^+$ T cells indicated robust antigen-specific immune responses in mice injected with Pt-Tu@NPs and Pt-Tu@NPs + αPD-L1 (Figures S76−S79). Moreover, IL-6 and IFN-γ were found to be elevated in Pt-Tu@NPs and Pt-Tu@NPs + αPD-L1 groups, thus indicating increased inflammation during immune responses (Figures S80 and S81).

Apart from the effective antigen presentation and functional $CD8^+$ T cells for the active immune response, successful immunotherapy requires the hot phenotype linked to a tumor microenvironment characterized by a "hot" phenotype. This phenotype is associated with the secretion of potent cytokines and chemokines, such as IFN-γ and IL-12, while simultaneously exhibiting a low abundance of immune suppressor cells and inhibitory factors like TGF-β and IL-10.[25] A reduction in the population of immune suppressor cells, including regulatory T cells (Tregs), alternatively activated M2 tumor-associated macrophages (M2-TAMs) cells, and myeloid-derived suppressor cells (MDSCs) was observed within the tumors of mice that received Pt-Tu@NPs treatment, as illustrated in Figure S82. Moreover, the administration of Pt-Tu@NPs resulted in an elevation of TNF-α, IL-12, and IFN-γ levels while concurrently reducing the concentration of TGF-β in the tumor tissues (Figure 6e). Furthermore, a sharp rise of potent cytokines and an evident decline of immune suppressor cells and factors in tumor tissues were found in the combined αPD-L1 therapy (Figures 6e and S82). These findings further supported the notion that Pt-Tu@NPs-mediated therapy could effectively reprogram the immunosuppressive tumor microenvironment and enhance the antitumor response, which was synergistically enhanced with the assistance of αPD-L1 therapy.

In addition, we employed healthy BALB/c mice as experimental subjects to assess the biocompatibility of the nanomedicines. Specifically, we investigated the impact of five consecutive administrations of standard blood indicators and liver function. Throughout the duration of the treatment, mice that were administered Pt@NPs, Tu@NPs, or Pt-Tu@NPs exhibited blood cell and liver enzyme levels that remained within the normal range (Figures S83 and S84). The data confirmed the safe application of these nanodrugs in cancer chemo-immunotherapy.

Recent studies reported that ICB-activated $CD8^+$ T cells could secrete higher amounts of IFN-γ capable of fostering IL-12 production from DCs, which in turn enhances the antitumor immunity of $CD8^+$ T cells.[26] Such a positive-feedback regulation magnifies the importance of IL-12 receptors on $CD8^+$ T cells, which can promote a strong response to IL-12. Endocytosis of Pt-Tu@NPs followed by intracellular degradation resulted in the release of the prodrug BC-Pt(IV), which can be reduced to generate coordinated butyrate (Figure 7a). Research indicates that butyrate upregulates the inhibitor of DNA binding 2 (ID2) through suppressing the activity of histone deacetylases (HDAC). ID2 can bind with the E-family of transcription factor protein (E2A) and antagonize its transcriptional activity, increasing the expression of IL-12 receptors and IFN-γ production, and thus boosting the antitumor reaction of cytotoxic T cells (Figure 7b).[27,28]

To probe the effect of Pt@NPs on the specific receptor signaling in $CD8^+$ T cells, mouse primary $CD8^+$ T cells were extracted for the analysis of IL-12 receptors expression with real-time fluorescent quantitative PCR (qRT-PCR) and the monitoring of $CD8^+$ T cell proliferation in vivo with the carboxyfluorescein diacetate succinimidyl ester (CFSE) method (Figure 7c). It showed that the prodrug BC-Pt(IV) indeed provoked higher expressions of IL-12Rβ1 and IL-12Rβ2 compared to those of the Pt(IV) treatment. Although all formulations raised the studied receptor levels to various degrees following the αCD3/CD28 stimulation, BC-Pt(IV), particularly in Pt@NPs group, led to a dramatically increased level of IL-12 receptors (Figure 7d). Moreover, IFN-γ in supernatants from BC-Pt(IV)-treated $CD8^+$ T cells noticeably increased, in both the absence and presence of αCD3/CD28 stimulation (Figure 7e). Intriguingly, Pt@NPs initiated a sudden increase in the secretion of IFN-γ, which might be attributed to high cellular uptake of the nanomedicine. For the in vivo CFSE tracking experiment, the proliferative response of CFSE-labeled, $CD45.2^+CD8^+$ T cells to different treatments was assayed 3 days after adoptive transfer of the T cells into recipient CD45.1 mice. The percentage of proliferative $CD45.2^+CD8^+$ T cells from the mouse lymph node in the PBS group was only 15.2%. In the presence of Pt(IV), the proliferation ratio of $CD8^+$ T cells was 26.2%, but an expansion in the number of transferred $CD8^+$ T (46.1%) cells was observed when BC-Pt(IV) was injected into recipient mice. However, it should be noted that in mice that received Pt@NPs, 90.2% of the CFSE-labeled $CD45.2^+CD8^+$ T cells proliferated, indicating a significant advantage of Pt@NPs in promoting $CD8^+$ T cell proliferation (Figures 7f,g and S85). These results provided evidence that Pt-Tu@NPs could facilitate the positive feedback between DCs and $CD8^+$ T cells, which would be a potential mechanism for greater T cell infiltration and tumor-killing effect of Pt-Tu@NPs as well as the improved response to the ICB combination.

CONCLUSIONS

In conclusion, a supramolecular nanomedicine was developed to amplify the chemotherapeutic efficacy and boost the synergistic efficacy of ICB therapy. For this, BC-Pt(IV) and Tu were loaded into the amphiphilic copolymers to produce a supramolecular nanomedicine that possessed the characteristics of prolonged blood circulation and high tumor accumulation. Pt-Tu@NPs strongly triggered the ER stress-mediated ICD of tumor cells, promoting DC maturation and T-cell infiltration, which boosted adaptive immunity. Furthermore, Pt-Tu@NPs synergized with αPD-L1 to improve the tumor infiltration of effector and cytotoxic T lymphocytes and provide a supportive microenvironment for antitumor immunity, thus resulting in impressive tumor suppression and antimetastasis effects. Pt@NPs prepared from CDDP which was axially coordinated by butyric acid were also proven to encourage the positive feedback between DCs and $CD8^+$ T cells. This pioneering work demonstrated that Pt-Tu@NPs remarkably enhanced the antitumor immunity and response to checkpoint blockade through the ER stress-mediated ICD, providing a promising nanomedicine platform for clinical applications in cancer chemoimmunotherapy.

METHODS

Cell Viability

The cytotoxicity effects of drugs against 4T1 cells were estimated by an MTT assay. Cells were seeded in 96-well plates (1×10^4 cells per well) and treated with varying concentrations of drugs or their

https://doi.org/10.1021/jacsau.3c00515
JACS Au 2023, 3, 3181−3193

nanoformulations for 48 h after attachment overnight. Cells grown in the medium alone were used as the control. Five replicate wells were used. At the end point, cells were incubated with 5.00 mg mL^{-1} filtered MTT solution (10 μL per well) at 37 °C in the dark for 4 h. After removing the MTT solution, the cells were washed with PBS three times. DMSO (100 μL per well) was added, and the solubilized formazan reagent was measured by a spectrophotometer at 570 nm wavelength.

Mice

Female BALB/c mice (5 weeks old) were obtained from Beijing Vital River Laboratory Animal Technology. Animal experiments were performed in accordance with the Institute of Laboratory Animal Resources guidelines. The program was approved by the Institutional Animal Care and Use Committee of Tsinghua University (Protocol No. 21-YGC1). For the breast tumor model, mice were injected into the mammary fat pad with 4T1 cells (1×10^5 cells in 100 μL cell suspension). After 12 days of tumor inoculation, the tumor size reached roughly 100 mm^3, and the mice were randomly divided into seven groups that were administered PBS, αPD-L1, CDDP, Pt@NPs, Tu@NPs, Pt-Tu@NPs, and Pt-Tu@NPs + αPD-L1. The doses of platinum-based drugs and nanomedicines were 2.00 mg CDDP per kg. Mice were administered with drugs five times through the caudal vein with an interval of 2 days. The tumor volume growth and body weight were monitored every 3 days. Tumor volume was calculated as (length) × $(\text{width})^2/2$. The TGI value was determined as (1-RTVx/RTVc) × 100%, where RTVx and RTVc represented the treatment and control group, respectively. Relative tumor volume (RTV) is the ratio of final tumor volume and initial volume. At the end time point, peripheral blood was collected from the retro-orbital sinus of anesthetized mice. The mice were killed, and lymph nodes, tumors, and lung tissues were obtained for the follow-up detection. The lung tissues were made into conventional hematoxylin and eosin sections for pathological observation.

Western Blotting

The 4T1 cells were homogenized in radio-immunoprecipitation assay lysis containing 10% phosphatase inhibitor and 1% protease inhibitor and then centrifuged at 14,000 × g at 4 °C for 10 min. The concentration of protein was analyzed by the bicinchoninic acid assay. Equivalent amounts of protein (40 mg) were loaded into 8%−12% sodium dodecyl sulfatepolyacrylamide gels and transferred onto polyvinylidene difluoride membranes. After blocking with 5% nonfat milk for 1.5 h at 20 °C, membranes were incubated with antiphospho-PERK, anti-PERK, antiphospho-EIF2S1, anti-EIF2S1, anti-ATF6, anticaspase-8, anticleaved-caspase-8, and anti-β-Actin at 4 °C overnight. After washing three times, the protein bands were incubated with horseradish peroxidase-conjugated secondary antibody for 1.5 h. Chemiluminescent signals were produced using an ECL kit and analyzed using the 4800Muti gel documentation system (Tanon, China).

Immunofluorescence

Cells were covered with ice-cold 100% methanol at −20 °C for 10 min and rinsed in 1 × PBS for 5 min. After blocking in 5% goat serum with 0.3% Triton X-100 for 1 h, cells were incubated with primary antibodies against CRT or HMGB1 (1:50) overnight at 4 °C. Rinsing was performed three times in 1 × PBS for 5 min each. Tumor slices were successively subjected to conventional dewaxing, antigen repair, and blocking operations and then incubated with primary and secondary antibodies. Nuclei were identified by DAPI staining. Cells were examined by an imaging system (NIS-Elements Viewer 5.21).

Statistical Analysis

All data are presented as the mean ± standard deviation (SD) and analyzed using Prism 8.0.1 software (GraphPad). Statistical significance was measured with one-way analysis of variance (ANOVA) followed by Turkey multiple comparison test. Significant differences were defined as $^*p < 0.05$, $^{**}p < 0.01$, $^{***}p < 0.001$.

ASSOCIATED CONTENT

Supporting Information

The Supporting Information is available free of charge at https://pubs.acs.org/doi/10.1021/jacsau.3c00515.

Materials, methods, chemical characterizations (NMR spectra, GPC, DLS), and additional experimental details (MTT, Western blot, flow cytometry, CLSM images, ELISA, biochemical analysis) (PDF)

AUTHOR INFORMATION

Corresponding Authors

Zhida Liu − *Shanxi Academy of Advanced Research and Innovation, Taiyuan 030032, P. R. China*; Email: zhida_liu@saari.org.cn

Marija Buljan − *Empa, Swiss Federal Laboratories for Materials Science and Technology, 9014 St. Gallen, Switzerland*; Email: Marija.Buljan@empa.ch

Xiaoyuan Chen − *Yong Loo Lin School of Medicine and College of Design and Engineering, National University of Singapore, Singapore 119074, Singapore*; orcid.org/0000-0002-9622-0870; Email: chen.shawn@nus.edu.sg

Guocan Yu − *MOE Key Laboratory of Bioorganic Phosphorus Chemistry & Chemical Biology, Department of Chemistry and School of Medicine, Tsinghua University, Beijing 100084, P. R. China*; orcid.org/0000-0003-1157-4184; Email: guocanyu@mail.tsinghua.edu.cn

Authors

Xinyang Yu − *MOE Key Laboratory of Bioorganic Phosphorus Chemistry & Chemical Biology, Department of Chemistry, Tsinghua University, Beijing 100084, P. R. China*

Shaolong Qi − *MOE Key Laboratory of Bioorganic Phosphorus Chemistry & Chemical Biology, Department of Chemistry, Tsinghua University, Beijing 100084, P. R. China*

Fangfang Cao − *Yong Loo Lin School of Medicine and College of Design and Engineering, National University of Singapore, Singapore 119074, Singapore*

Kai Yang − *MOE Key Laboratory of Bioorganic Phosphorus Chemistry & Chemical Biology, Department of Chemistry, Tsinghua University, Beijing 100084, P. R. China*

Hongjian Li − *School of Medicine, Tsinghua University, Beijing 100084, P. R. China*

Kun Peng − *School of Medicine, Tsinghua University, Beijing 100084, P. R. China*

Bing Bai − *MOE Key Laboratory of Bioorganic Phosphorus Chemistry & Chemical Biology, Department of Chemistry, Tsinghua University, Beijing 100084, P. R. China*

Complete contact information is available at: https://pubs.acs.org/10.1021/jacsau.3c00515

Author Contributions

X.Y., B.M., X.C., and G.Y. conceived and designed the research. X.Y., S.Q., F.C., and K.Y. prepared and characterized the nanoformulations. X.Y., H.L., K.P., Z.L., and B.B. performed in vitro and in vivo studies. X.Y., H.L., S.Q., K.Y., K.P., and B.B. analyzed the data. X.Y., Z.L., B.M., X.C., and G.Y. cowrote and revised the paper. CRediT: **Zhida Liu** investigation, writing-review & editing.

Notes

The authors declare no competing financial interest.

https://doi.org/10.1021/jacsau.3c00515
JACS Au 2023, 3, 3181−3193

■ ACKNOWLEDGMENTS

This work was supported by the National Natural Science Foundation of China (22175107), the National Key Research and Development Program of China (2021YFA0910100), the Vanke Special Fund for Public Health and Health Discipline Development, Tsinghua University (2022Z82WKJ005, 2022Z82WKJ013), the Tsinghua University Spring Breeze Fund (2021Z99CFZ007), Shanxi Provincial Science and Technology Innovation Young talent team Program (202204051001029), and Shanxi Provincial Key Research and Development Program (202102140601020).

■ REFERENCES

(1) Irvine, D. J.; Dane, E. L. Enhancing cancer immunotherapy with nanomedicine. *Nat. Rev. Immunol.* **2020**, *20*, 321−334.
(2) Chen, D.; Mellman, I. Elements of cancer immunity and the cancer-immune set point. *Nature* **2017**, *541*, 321−330.
(3) Bruni, D.; Angell, H. K.; Galon, J. The immune contexture and Immunoscore in cancer prognosis and therapeutic efficacy. *Nat. Rev. Cancer* **2020**, *20*, 662−680.
(4) Qian, Q.; Zhu, L.; Zhu, X.; Sun, M.; Yan, D. Drug-polymer hybrid macromolecular engineering: degradable PEG integrated by platinum(IV) for cancer therapy. *Matter* **2019**, *6*, 1618−1630.
(5) De Biasi, A. R.; Villena-Vargas, J.; Adusumilli, P. S. Cisplatin-Induced Antitumor Immunomodulation: A Review of Preclinical and Clinical Evidence. *Clin. Cancer Res.* **2014**, *20*, 5384−5391.
(6) Mai, H. Q.; Chen, Q. Y.; Chen, D.; Hu, C.; Yang, K.; Wen, J.; Li, J.; Shi, Y. R.; Jin, F.; Xu, R.; Pan, J.; Qu, S.; Li, P.; Hu, C.; Liu, Y. C.; Jiang, Y.; He, X.; Wang, H. M.; Lim, W. T.; Liao, W.; He, X.; Chen, X.; Liu, Z.; Yuan, X.; Li, Q.; Lin, X.; Jing, S.; Chen, Y.; Lu, Y.; Hsieh, C. Y.; Yang, M. H.; Yen, C. J.; Samol, J.; Feng, H.; Yao, S.; Keegan, P.; Xu, R. H. Toripalimab or placebo plus chemotherapy as first-line treatment in advanced nasopharyngeal carcinoma: a multicenter randomized phase 3 trial. *Nat. Med.* **2021**, *27*, 1536−1543.
(7) Li, W.; Yang, J.; Luo, L.; Jiang, M.; Qin, B.; Yin, H.; Zhu, C.; Yuan, X.; Zhang, J.; Luo, Z.; Du, Y.; Li, Q.; Lou, Y.; Qiu, Y.; You, J. Targeting photodynamic and photothermal therapy to the endoplasmic reticulum enhances immunogenic cancer cell death. *Nat. Commun.* **2019**, *10*, 3349.
(8) Limagne, E.; Nuttin, L.; Thibaudin, M.; Jacquin, E.; Aucagne, R.; Bon, M.; Revy, S.; Barnestein, R.; Ballot, E.; Truntzer, C.; Derangère, V.; Fumet, J. D.; Latour, C.; Rébé, C.; Bellaye, P. S.; Kaderbhaï, C. G.; Spill, A.; Collin, B.; Callanan, M. B.; Lagrange, A.; Favier, L.; Coudert, B.; Arnould, L.; Ladoire, S.; Routy, B.; Joubert, P.; Ghiringhelli, F. MEK inhibition overcomes chemoimmunotherapy resistance by inducing CXCL10 in cancer cells. *Cancer Cell* **2022**, *40*, 136−152.e112.
(9) Yoo, J.; Mashalidis, E. H.; Kuk, A. C. Y.; Yamamoto, K.; Kaeser, B.; Ichikawa, S.; Lee, S.-Y. GlcNAc-1-P-transferase−tunicamycin complex structure reveals basis for inhibition of N-glycosylation. *Nat. Struct. Mol. Biol.* **2018**, *25*, 217−224.
(10) Martins, I.; Kepp, O.; Schlemmer, F.; Adjemian, S.; Tailler, M.; Shen, S.; Michaud, M.; Menger, L.; Gdoura, A.; Tajeddine, N.; Tesniere, A.; Zitvogel, L.; Kroemer, G. Restoration of the immunogenicity of cisplatin-induced cancer cell death by endoplasmic reticulum stress. *Oncogene* **2011**, *30*, 1147−1158.
(11) Pajic, M.; Blatter, S.; Guyader, C.; Gonggrijp, M.; Kersbergen, A.; Küçükosmanoğlu, A.; Sol, W.; Drost, R.; Jonkers, J.; Borst, P.; Rottenberg, S. Selected Alkylating Agents Can Overcome Drug Tolerance of G0-like Tumor Cells and Eradicate BRCA1-Deficient Mammary Tumors in Mice. *Clin. Cancer Res.* **2017**, *23*, 7020−7033.
(12) Ajani, J. A.; Abramov, M.; Bondarenko, I.; Shparyk, Y.; Gorbunova, V.; Hontsa, A.; Otchenash, N.; Alsina, M.; Lazarev, S.; Feliu, J.; Elme, A.; Esko, V.; Abdalla, K.; Verma, U.; Benedetti, F.; Aoyama, T.; Mizuguchi, H.; Makris, L.; Rosati, G.; DIGEST Study Group. A phase III trial comparing oral S-1/cisplatin and intravenous 5-fluorouracil/cisplatin in patients with untreated diffuse gastric cancer. *Ann. Oncol.* **2017**, *28*, 2142−2148.
(13) Zhang, M.; Song, R.; Liu, Y.; Yi, Z.; Meng, X.; Zhang, J.; Tang, Z.; Yao, Z.; Liu, Y.; Liu, X. Calcium-Overload-Mediated Tumor Therapy by Calcium Peroxide Nanoparticles. *Chem.* **2019**, *5*, 2171−2182.
(14) Johnstone, T. C.; Suntharalingam, K.; Lippard, S. J. The Next Generation of Platinum Drugs: Targeted Pt(II) Agents, Nanoparticle Delivery, and Pt(IV) Prodrugs. *Chem. Rev.* **2016**, *116*, 3436−3486.
(15) Zhang, W.; Du, X. F.; Liu, B.; Li, C.; Long, J.; Zhao, M. X.; Yao, Z.; Liang, X. J.; Lai, Y. Engineering Supramolecular Nanomedicine for Targeted Near Infrared-triggered Mitochondrial Dysfunction to Potentiate Cisplatin for Efficient Chemophototherapy. *ACS Nano* **2022**, *16*, 1421−1435.
(16) Zhang, Y.; Ma, S.; Liu, X.; Xu, Y.; Zhao, J.; Si, X.; Li, H.; Huang, Z.; Wang, Z.; Tang, Z.; Song, W.; Chen, X. Supramolecular Assembled Programmable Nanomedicine As In Situ Cancer Vaccine for Cancer Immunotherapy. *Adv. Mater.* **2021**, *33*, No. e2007293.
(17) Ma, X.; Zhao, Y. Biomedical Applications of Supramolecular Systems Based on Host-Guest Interactions. *Chem. Rev.* **2015**, *115*, 7794−7839.
(18) Wang, Z.; Sun, C.; Yang, K.; Chen, X.; Wang, R. Cucurbituril-Based Supramolecular Polymers for Biomedical Applications. *Angew. Chem., Int. Ed.* **2022**, *61*, No. e202206763.
(19) Gong, F.; Xu, J.; Liu, B.; Yang, N.; Cheng, L.; Huang, P.; Wang, C.; Chen, Q.; Ni, C.; Liu, Z. Nanoscale CaH_2 materials for synergistic hydrogen-immune cancer therapy. *Chem.* **2022**, *8*, 268−286.
(20) Galluzzi, L.; Senovilla, L.; Zitvogel, L.; Kroemer, G. The secret ally: immunostimulation by anticancer drugs. *Nat. Rev. Drug Discovery* **2012**, *11*, 215−233.
(21) Gardai, S. J.; McPhillips, K. A.; Frasch, S. C.; Janssen, W. J.; Starefeldt, A.; Murphy-Ullrich, J. E.; Bratton, D. L.; Oldenborg, P. A.; Michalak, M.; Henson, P. M. Cell-Surface Calreticulin Initiates Clearance of Viable or Apoptotic Cells through trans-Activation of LRP on the Phagocyte. *Cell* **2005**, *123*, 321−334.
(22) Li, C.; Bi, Y.; Li, Y.; Yang, H.; Yu, Q.; Wang, J.; Wang, Y.; Su, H.; Jia, A.; Hu, Y.; Han, L.; Zhang, J.; Li, S.; Tao, W.; Liu, G. Dendritic cell MST1 inhibits Th17 differentiation. *Nat. Commun.* **2017**, *8*, 14275.
(23) Trinchieri, G. Interleukin-12 and the regulation of innate resistance and adaptive immunity. *Nat. Rev. Immunol.* **2003**, *3*, 133−146.
(24) Liu, X.; Liu, L.; Ren, Z.; Yang, K.; Xu, H.; Luan, Y.; Fu, K.; Guo, J.; Peng, H.; Zhu, M.; Fu, Y. X. Dual Targeting of Innate and Adaptive Checkpoints on Tumor Cells Limits Immune Evasion. *Cell Rep.* **2018**, *24*, 2101−2111.
(25) Martin, J. D.; Cabral, H.; Stylianopoulos, T.; Jain, R. K. Improving cancer immunotherapy using nanomedicines: progress, opportunities and challenges. *Nat. Rev. Clin. Oncol.* **2020**, *17*, 251−266.
(26) Garris, C. S.; Arlauckas, S. P.; Kohler, R. H.; Trefny, M. P.; Garren, S.; Piot, C.; Engblom, C.; Pfirschke, C.; Siwicki, M.; Gungabeesoon, J.; Freeman, G. J.; Warren, S. E.; Ong, S.; Browning, E.; Twitty, C. G.; Pierce, R. H.; Le, M. H.; Algazi, A. P.; Daud, A. I.; Pai, S. I.; Zippelius, A.; Weissleder, R.; Pittet, M. J. Successful Anti-PD-1 Cancer Immunotherapy Requires T Cell-Dendritic Cell Crosstalk Involving the Cytokines IFN-γ and IL-12. *Immunity* **2018**, *49*, 1148−1161.e1147.
(27) Reina-Campos, M.; Scharping, N. E.; Goldrath, A. W. $CD8^+$ T cell metabolism in infection and cancer. *Nat. Rev. Immunol.* **2021**, *21*, 718−738.
(28) He, Y.; Fu, L.; Li, Y.; Wang, W.; Gong, M.; Zhang, J.; Dong, X.; Huang, J.; Wang, Q.; Mackay, C. R.; Fu, Y. X.; Chen, Y.; Guo, X. Gut microbial metabolites facilitate anticancer therapy efficacy by modulating cytotoxic $CD8^+$ T cell immunity. *Cell Metab.* **2021**, *33*, 988−1000.e1007.

https://doi.org/10.1021/jacsau.3c00515
JACS Au 2023, 3, 3181−3193